OPEN ACCESS

University of BRISTOL

Peer reviewed version

Link to published version (if available):
10.1021/acs.jpcb.6b01459

Link to publication record in Explore Bristol Research
PDF-document

University of Bristol - Explore Bristol Research
General rights

Unified Model of Nanosecond Charge Recombination in Closed Reaction Centers from *Rhodobacter sphaeroides*: Role of Protein Polarization Dynamics

K. Dubas,[1] M. Baranowski,[2] A. Podhorodecki,[2] M.R. Jones,[3] K. Gibasiewicz[1]*

[1] Department of Physics, Adam Mickiewicz University, ul. Umultowska 85, 61-614 Poznań, Poland.

[2] Department of Experimental Physics, Wroclaw University of Technology, Wybrzeze Wyspianskiego 27, 50-370 Wroclaw, Poland

[3] School of Biochemistry, Medical Sciences Building, University of Bristol, University Walk, Bristol, BS8 1TD, UK

* Corresponding author; e-mail: krzyszgi@amu.edu.pl; Tel: +48 61 8296370

Abstract

Ongoing questions surround the influence of protein dynamics on rapid processes such as biological electron transfer. Such questions are particularly addressable in light-activated systems. In *Rhodobacter sphaeroides* reaction centers, charge recombination or back electron transfer from the reduced bacteriopheophytin, H_A^-, to the oxidized dimeric bacteriochlorophyll, P^+, may be monitored by both transient absorption spectroscopy and transient fluorescence spectroscopy. Signals measured with both these techniques decay in a similar three-exponential fashion with lifetimes of ~0.6-0.7 ns, ~2-4 ns, and ~10-20 ns, revealing the complex character of this electron transfer reaction. In this study a single kinetic model was developed to connect lifetime and amplitude data from both techniques. The model took into account the possibility that electron transfer from H_A^- to P^+ may occur with transient formation of the state $P^+B_A^-$. As a result it was possible to model the impact of nanosecond protein relaxation on the free energy levels of both $P^+H_A^-$ and $P^+B_A^-$ states relative to that of the singlet excited state of P, P*. Surprisingly, whereas the free energy gap between P* and $P^+H_A^-$ increased with time in response to protein reorganization, the free energy gap between P* and $P^+B_A^-$ decreased. This finding may be accounted for by a gradual polarization of the protein environment which stabilizes the state $P^+H_A^-$ and destabilizes the state $P^+B_A^-$, favoring productive charge separation over unproductive charge recombination.

Introduction

The appearance of electrical charges and their transfer inside a protein is expected to trigger a dielectric response from the protein environment.[1] It is well known that in the case of photosynthetic reaction centers (RCs), pigment-protein complexes specialized in transferring electrons across a biological membrane in response to light absorption, the lifetimes of the measureable electron transfer reactions extend from picoseconds (primary electron transfer) to milliseconds (last steps of forward electron transfer) or seconds (membrane-spanning charge recombination reactions).[2] However, the dynamics of the dielectric response of the reaction center protein to the individual electron transfer events remains poorly understood.

In purple bacterial reaction centers such as that from *Rhodobacter* (*Rba.*) *sphaeroides*, the ultrafast (~3 ps) primary charge separation reaction comprises electron transfer from the excited primary donor P* (a dimer of bacteriochlorophyll *a* (BChl)) to the primary acceptor H_A (a bacteriopheophytin (BPhe)), leading to formation of the state $P^+H_A^-$ (Fig. 1A, B). This reaction has been studied intensively as it is crucial for efficient conversion of excitation energy into chemical energy,[3] and it has been proposed that protein dynamics play an important role in this ultrafast reaction.[4] However, the efficiency of energy conversion depends not only on the rate and yield of this forward reaction but also on the rates and yields of unwanted charge recombination reactions. Among the latter the most critical is the primary charge recombination process, $P^+H_A^- \rightarrow PH_A$, which leads to the loss of energy initially captured through light absorption and stored in the form of the primary charge separated state. It was proposed that an important factor preventing this wasteful charge recombination step is protein reorganization triggered by appearance of the charges on P^+ and H_A^-.[5] The protein response quickly shifts the free energy level of the state $P^+H_A^-$ down away from the state $P^+B_A^-$ (Fig. 1C), the latter being a short-lived intermediate that, in addition to facilitating electron transfer from P* to H_A, also could facilitate charge recombination from H_A^- to P^+.[5-9] The B_A cofactor is a BChl located between the P BChl dimer and the H_A BPhe (Fig. 1A). This increase in free energy gap is important since otherwise the state $P^+B_A^-$, initially almost isoenergetic with $P^+H_A^-$,[5, 10,11] could be efficiently repopulated from $P^+H_A^-$. As a consequence, since the intrinsic lifetime of $P^+B_A^- \rightarrow PB_A$ charge recombination is of the same order of magnitude (200-700 ps)[12-15] as the lifetime of the next forward electron transfer step from H_A^- to the quinone Q_A (~200 ps),[16] the initially accumulated energy would be lost with a significant probability. Accordingly, relaxation of the state $P^+H_A^-$ together with relatively slow direct $P^+H_A^- \rightarrow PH_A$ charge recombination (of the order of 20 ns;[2,11,17] Fig. 1B) protects

2

the system against wasteful charge recombination. Studies of mutant RCs with decreased free energy gap between $P^+B_A^-$ and $P^+H_A^-$ have shown that the reaction of $P^+H_A^- \rightarrow PH_A$ charge recombination, via the state $P^+B_A^-$, competes with forward electron transfer from H_A^- to Q_A.[5,14,18]

In order to study $P^+H_A^- \rightarrow PH_A$ charge recombination it is necessary to block electron transfer from H_A^- to the next acceptor, the Q_A ubiquinone. This is usually achieved by either removal or reduction of Q_A, and such reaction centers are described as being in a "closed" state).[5,11] One of the first experimental manifestations of protein relaxation occurring on the time scale of charge recombination in closed *Rba. sphaeroides* RCs was the detection of multiexponential decay of fluorescence from P* (originating from P* repopulated from the states $P^+B_A^-/P^+H_A^-$; Fig. 1A).[19] However during two decades subsequent to this finding there was a lack of experimental transient absorption data that could clearly support the idea of protein relaxation in purple bacterial RCs. Counter to this interpretation, a large body of evidence indicated that transient absorption signals from closed RCs, achieved by both reduction and removal of Q_A, decayed monoexponentially with a lifetime of 12-15 ns at room temperature.[2,17] Only recently it was well documented that transient absorption signals in closed, Q_A-reduced RCs decay in a multiexponential fashion[8,11] with lifetimes similar to those observed in time-resolved fluorescence studies (< 1 ns, 2-4 ns and 10-20 ns). In RCs with Q_A reduced the two fastest components are dominant. RCs with Q_A removed showed a significantly slower decay dominated by a >10 ns component.[5,8] The common use of RCs without Q_A, together with lower temporal resolution of older transient absorption experiments, was probably the reason why non-monoexponential charge recombination was not detected in many previous studies.

In this contribution we combined new and old data on multiexponential decay of P* fluorescence with recent data on a multiexponential decay of $P^+H_A^-$ measured by transient absorption, both in Q_A-reduced RCs.[11,19,20] The determination of similar sets of three lifetimes from both of these techniques prompted us to propose a unified model for charge recombination that includes an active role of protein polarization dynamics.

Materials and Methods

Charge recombination reaction was studied by time-resolved fluorescence in wild-type *Rba. sphaeroides* RCs that were purified according to a procedure described previously.[21] Before the experiments, isolated RCs were diluted in 15 mM Tris buffer (pH 8.2), containing 0.025% LDAO (*N,N*–dimethyldodecylamine-*N*-oxide) to a final optical density of OD_{800nm},

$_{1cm} \approx 0.1$. In order to keep the RCs in the closed state (i.e. with Q_A reduced), 10 mM sodium ascorbate was added.[11] During the experiment, the sample was kept in a stirred quartz cell (1 cm path length).

An instrument equipped with a streak camera was used to measure time-resolved fluorescence.[22] Samples were excited by 150 fs laser pulses of 800 nm wavelength provided by Ti:Sapphire oscillators pumped by a high stability Nd:YVO4 DPSS CW laser. The standard pulse repetition rate (76 MHz) of our Ti:Sapphire oscillators was reduced to 4.75 MHz by a pulse-picker in order to provide an appropriate time between pulses. The detection system for fluorescence decay time experiments consisted of a Hamamatsu S1 streak camera coupled to a 0.3 m focal length monochromator. The fluorescence decay was detected with ~0.5-ns temporal resolution in a 50 ns time window.

Time-resolved fluorescence traces were fitted with three exponential functions, $Fl(t) = \sum_{i=1}^{3} F_i \exp\left(-\frac{t}{\tau_i}\right)$, using the program Origin. The fits were performed without convolution with the instrumental response function. This approach is justified because the previously published transient absorption kinetics characterized by a similar temporal resolution of ~0.5 ns,[11] analyzed in this study together with the fluorescence kinetics using the unified model, were also performed without convolution with the instrumental response function. The reference data of decay of absorption change was fitted with the function $\sum_{i=1}^{3} A_i \exp\left(-\frac{t}{\tau_i}\right) + A_4$. Transient absorption signals were measured at 690 nm (signal from H_A^-) in ref. 11 or at wavelengths of 369, 420, 454, 668 nm (from 0 to 1 ns) combined with 970 nm (from 0 to 80 ns; signal mostly from P^+) in ref. 20. Average fluorescence and absorption decay times were calculated as $\tau_{av} = \sum_{i=1}^{3} \tau_i F_i$ and $\tau_{av} = \sum_{i=1}^{3} \tau_i A_i$, respectively. Steady-state fluorescence spectra were measured using a CCD InGAs Camera.

Results and Discussion

Fig. 1D presents the fluorescence spectrum of closed (with Q_A^-) *Rba. sphaeroides* RCs excited at 800 nm, overlaid on the absorbance spectrum of the same complex; emission was obtained to the red of the lowest energy P absorbance band at 865 nm. The shoulder on the blue side of the fluorescence spectrum is probably due to a very small amount of free pigment and/or by the shape of the response function of the detecting system. Fig. 2 shows the fluorescence decay signal integrated over a part of the P^* emission band near the maximum from ~920 to ~940 nm, again following excitation at 800 nm. Superimposed on the decay trace is the best three-exponential free fit with lifetimes of 0.63, 2.4, and 9.6 ns (Fig. 2). No

faster fluorescence components were detected due to the limited temporal resolution of the instrument, which was similar to that of previous transient absorption measurements (~0.5 ns). The multiexponential character of this decay of P* fluorescence was previously attributed to a combined effect of charge recombination and protein relaxation.[11,19]

Fig. 3 compares the best free fit of the decay of P* fluorescence (blue trace) with the fit made using lifetimes of 0.7, 3.8 and 17.7 ns obtained from a previous transient absorption study (dashed black trace).[11] As is evident from the way these fit curves superimpose, and the similarity of the residuals from these fits shown in Fig. 3 (traces a and b, respectively), the difference between these two fits was not significant. The best fit to the previous transient absorption data[11] using the 0.7, 3.8 and 17.7 ns lifetimes is also shown in Fig. 3 (red trace). The divergence from the fits to the fluorescence data is due to the different relative amplitudes for the respective components. In the fluorescence data the fastest component dominated (F_1 = 0.73 or 0.79), whereas in transient absorption data the intermediate component had the largest amplitude (A_2 = 0.48). This difference in relative amplitudes is due to the fact that the amplitude of the fluorescence signal is proportional to the transient concentration of the P* state formed by charge recombination whereas the amplitude of the absorption signal is proportional to the transient concentration of the state $P^+H_A^-$ (with admixture of the state $P^+B_A^-$; most of the ΔA signal at 690 nm comes from H_A^- and B_A^-).[9,23] Thus, a gradual increase over time of the free energy gap between P* and $P^+H_A^-$ due to protein relaxation is expected to decrease the amplitude of the signal from P* faster than that of the signal from H_A^-/B_A^- (compare the transient absorption and fluorescence traces in Fig. 3).

Lifetimes and amplitudes obtained in the three-exponential fits of charge recombination measured either by time-resolved fluorescence or time-resolved absorption are compared in Table 1. Parameters obtained from the free fit of the fluorescence decay data (set A in Table 1) were similar to those obtained in a previous study by Woodbury and Parson[19] (set D in Table 1), the main variance being a difference in the calculated average fluorescence lifetime (1.61 vs. 2.45 ns, respectively). Two sets of parameters obtained from free fits of transient absorption data obtained in recent studies[11, 20] were also similar to one another (sets F and G in Table 1) and the lifetime parameters were not markedly different from those estimated from the fluorescence measurements. Parameter sets B and C were obtained after fixing the lifetimes taken from transient absorption experiments (ref. 11 and ref 20, respectively), and set E results from old fluorescence decay data[19] but fitted with fixed lifetimes taken from transient absorption studies.[11] As will be shown below the differences between the respective sets of parameters (A-E and F-G), and in particular the differences

between lifetime parameters in all the sets (A-G), were not critical for the conclusions drawn in this study. The similarity in the lifetime parameters found in transient fluorescence and transient absorption experiments justifies an assumption that in model calculations one set of lifetimes should be sufficient to describe the processes underlying the results of both types of experiment.

A mathematical model allowing calculation of the free energy levels of the states $P^+B_A^-$ and $P^+H_A^-$ relative to that of P^* on the basis of fluorescence decay parameters (Tab. 1; sets A-E) and biphasic protein relaxation parameters τ_{12} and τ_{23} (Tab. 1) estimated earlier on the basis of transient absorption measurements[11] is presented in the Supporting Information. This is an extension of a model developed previously and applied to simulation of the temporal evolution of the free energy gap between the states $P^+B_A^-$ and $P^+H_A^-$ based exclusively on data from a previous transient absorption study.[11] The output from the extended model were populations of the states P^*, $P^+B_A^-$ and $P^+H_A^-$ and free energy gaps (ΔG) between these states in three relaxation states of the protein (Tab. 2).

Example results of the model calculations are collected in Table 2 and the results for two of the parameter sets (A and B) are presented graphically in Fig. 4. In all cases the free energy gap between the states $P^+B_A^-$ and $P^+H_A^-$ at a given relaxation state of the protein was adopted from a recent transient absorption study,[11] and thus the added value of the current modeling is an estimation of the temporal resolution of the free energy gap between P^* and $P^+B_A^-$. Careful comparison of the sets of results in Table 2 (columns 4-7) and Fig. 4 (A and B) leads to conclusion that, whichever set of fit parameters one puts into the model calculations, the temporal evolution of the free energy levels of the states $P^+B_A^-$ and $P^+H_A^-$ relative to that of P^* is qualitatively the same. In all cases the gap between $P^+H_A^-$ and P^* increases with time, and the gap between $P^+B_A^-$ and P^* decreases with time on a (sub)nanosecond time scale.

The observed effect may be explained in the following way (see the Table of Contents graphic for a visualisation). Formation of the initial unrelaxed form of states $P^+B_A^-$ and $P^+H_A^-$, $(P^+B_A^-)_1$ and $(P^+H_A^-)_1$, occurs very quickly, within a few picoseconds, this time being beyond the temporal resolution of the applied instrumentation. Since the initial free energy gap between $(P^+B_A^-)_1$ and $(P^+H_A^-)_1$ is small (ΔG_1 = 8 meV, Table 2), there is only a small population excess of $(P^+H_A^-)_1$ over $(P^+B_A^-)_1$ (see population probabilities P_1 and $P_1{}'$ in Table 2). This situation only slightly favors protein polarization with positive poles directed towards H_A^-/H_A and negative poles directed towards P^+ and B_A^-/B_A. The change in distribution of charge within the protein associated with a mixture of $(P^+B_A^-)_1$ and $(P^+H_A^-)_1$ triggers the first phase of protein reorganization that corresponds to lifetime τ_{12} (Table 1). This 0.6-0.7 ns

6

process comprises a partial polarization of the protein environment of the cofactors resulting in partially relaxed states $(P^+B_A^-)_2$ and $(P^+H_A^-)_2$; this polarization can be envisaged as the reorientation of positive partial charges directed towards H_A^-/H_A and negative partial charges directed towards P^+. When the free energy gap between $P^+B_A^-$ and $P^+H_A^-$ increases due to this partial polarization ($\Delta G_2 = 92$ meV, Table 2), the population excess of $(P^+H_A^-)_2$ over $(P^+B_A^-)_2$ becomes large (see P_2 and $P_2{'}$ in Table 2). This results in the protein polarization becoming stronger (second phase of protein reorganization, τ_{23}) with a further increase in the relative population of a fully relaxed $(P^+H_A^-)_3$ state over $(P^+B_A^-)_3$. A consequence of the protein polarization is that the negative poles near B_A shift the free energy level of the state $P^+B_A^-$ up towards P^*, due to electrostatic repulsive interaction with the negative charge on B_A^-, whereas the positive poles stabilize the state $P^+H_A^-$ due to the attractive interaction with the negatively charged H_A^-. Thus stabilization of $P^+H_A^-$ is accompanied by destabilization of $P^+B_A^-$.

Naturally, this qualitative explanation of the observed effect does not solve the question of the nature of the protein polarization. Is it simply nuclear reorganization of dipolar groups of amino acids in the vicinity of B_A and H_A, or one or more protonation/deprotonation events occurs somewhere between B_A and H_A? Systematic studies similar to those performed in this work on WT RCs are needed on mutant RCs with altered polarity or charges around B_A and H_A to address this question.

Supporting Information Available

Supporting Information, available via the Internet at http://pubs.acs.org, presents a mathematical model allowing calculation of the free energy levels of the states $P^+B_A^-$ and $P^+H_A^-$ relative to that of P^* on the basis of fluorescence decay parameters (Tab. 1; sets A-E) and biphasic protein relaxation parameters τ_{12} and τ_{23} (Tab. 1) estimated earlier on the basis of transient absorption measurements.[11]

References

(1) Frauenfelder, H. *The Physics of Proteins: An Introduction to Biological Physics and Molecular Biophysics;* Springer-Verlag: New York, 2011.

(2) Volk, M.; Ogrodnik, A.; Michel-Beyerle, M. E. The Recombination Dynamics of the Radical Pair P^+H^- in External Magnetic and Electric Fields. *In*: Blankenship, R. E.; Madigan, M. T.; Bauer, C. E. *Anoxygenic Photosynthetic Bacteria*; Kluwer Academic Publishers: Dordrecht, Boston, London, The Netherlands, 1995.

(3) Parson, W. W.; Warshel, A. Mechanism of Charge Separation in Purple Bacterial Reaction Centers. *In*: Hunter, C. N.; Daldal, F.; Thurnauer, M. C.; Beatty, J. T. *The Purple Phototropic Bacteria*; Springer Netherlands, 2009.

(4) Wang, H.; Lin, S.; Allen, J. P.; Williams, J. A. C.; Blankert, S.; Laser, C.; Woodbury, N. W. Protein Dynamics Control the Kinetics of Initial Electron Transfer in Photosynthesis. *Science* **2007**, 316 (5825), 747-750.

(5) Wang, H.; Hao, Y.; Jiang, Y.; Lin, S.; Woodbury, N. W. The Role of Protein Dynamics in Guiding Electron Transfer Pathways in Reaction Centers from Rhodobacter sphaeroides. *J. Phys. Chem. B* **2012**, 116, 711-717.

(6) Kirmaier, C.; Holten, D. Temperature Effects on the Ground State Absorption Spectra and Electron Transfer Kinetics of Bacterial Reaction Centers; *In*: Breton, J.; Vermeglio, A. *The Photosynthetic Bacterial Reaction Center*; Springer US, 1988.

(7) Arlt, T.; Schmidt, S.; Kaiser, W.; Lauterwasser, C.; Meyer, M.; Scheer, H.; Zinth, W. The Accessory Bacteriochlorophyll: a Real Electron Carrier in Primary Photosynthesis. *Proc. Natl. Acad. Sci. U.S.A.* **1993,** 90 (24), 11757-11761.

(8) Gibasiewicz, K.; Pajzderska, M. Primary Radical Pair P$^+$H$^-$ Lifetime in Rhodobacter sphaeroides with Blocked Electron Transfer to Q$_A$. Effect of o-Phenanthroline. *J. Phys. Chem. B* **2008,** 112 (6), 1858-1865.

(9) Zhu, J. Y.; van Stokkum, H. M.; Paparelli, L.; Jones, M. R.; Groot, M. L. Early Bacteriopheophytin Reduction in Charge Separation in Reaction Centers of Rhodobacter sphaeroides. *Biophys. J.* **2013**, 104 (11), 2493-2502.

(10) Guo, Z.; Woodbury, N. W.; Pan, J.; Lin, S. Protein Dielectric Environment Modulates the Electron-Transfer Pathway in Photosynthetic Reaction Centers. *Biophys. J.* **2012**, 103, 1979–1988.

(11) Gibasiewicz, K.; Pajzderska, M.; Dobek, A.; Karolczak, J.; Burdziński, G.; Brettel, K.; Jones, M. R. Analysis of the Temperature-Dependence of P$^+$H$_A^-$ Charge Recombination in the Rhodobacter sphaeroides Reaction Center Suggests Nanosecond Temperature-Independent Protein Relaxation. *Phys. Chem. Chem. Phys.* **2013**, 15, 16321-16333.

(12) Schmidt, S.; Arlt, T.; Hamm, P.; Huber, H.; Nägele, T.; Wachtveitl, J.; Meyer, M.; Scheer, H.; Zinth, W. Energetics of the Primary Electron Transfer Reaction Revealed by Ultrafast Spectroscopy on Modified Bacterial Reaction Centers. *Chem. Phys. Lett.* **1994**, 223, 116-120.

(13) Kirmaier, C.; Laporte, L.; Schenck, C. C.; Holten, D. The Nature and Dynamics of the Charge-Separated Intermediate in Reaction Centers in which Bacteriochlorophyll Replaces the Photoactive Bacteriopheophytin. 2. The Rates and Yields of Charge Separation and Recombination. *J. Phys. Chem.* **1995**, 99 (21), 8910-8917.

(14) Heller, B. A.; Holten, D.; Kirmaier, C. Effects of Asp Residues Near the L-Side Pigments in Bacterial Reaction Centers. *Biochemistry* **1996**, 35, 15418- 15427.

(15) Katilius, E.; Turanchik, T.; Lin, S.; Taguchi, A. K. W.; Woodbury, N. W. J. B-Side Electron Transfer in a Rhodobacter sphaeroides Reaction Center Mutant in which the B-Side Monomer Bacteriochlorophyll is Replaced with Bacteriopheophytin. *J. Phys. Chem. B* **1999**, 103 (35), 7385-7389.

(16) Woodbury, N. W. T.; Allen, J. P. The Pathway, Kinetics and Thermodynamics of Electron Transfer in Wild Type and Mutant Reaction Centers of Purple Nonsulfur Bacteria. *In*: Blankenship, R. E.; Madigan, M. T.; Bauer, C. E. *Anoxygenic Photosynthetic Bacteria*; Kluwer Academic Publishers: Dordrecht, Boston, London, The Netherlands, 1995.

(17) Tang, C. K.; Williams, J. C.; Taguchi, A. K. W.; Allen, J. P.; Woodbury, N. W. P+HA- Charge Recombination Reaction Rate Constant in Rhodobacter sphaeroides Reaction Centers is Independent of the P/P+ Midpoint Potential. *Biochemistry* **1999**, *38*, 8794-8799.

(18) Gibasiewicz, K.; Pajzderska, M.; Potter, J. A.; Fyfe, P. K.; Dobek, A.; Brettel, K.; Jones, M. R. Mechanism of Recombination of the $P^+H_A^-$ Radical Pair in Mutant Rhodobacter sphaeroides Reaction Centers with Modified Free Energy Gaps Between $P^+B_A^-$ and $P^+H_A^-$. *J. Phys. Chem. B* **2011,**115 (44), 13037-13050.

(19) Woodbury, N. W. T.; Parson, W. W. Nanosecond Fluorescence from Isolated Photosynthetic Reaction Centers of Rhodopseudomonas sphaeroides. *Biochim. Biophys. Acta* **1984**, 767 (2), 345-361.

(20) Gibasiewicz, K.; Pajzderska, M.; Ziółek, M.; Karolczak, J.; Dobek, A. Internal Electrostatic Control of the Primary Charge Separation and Recombination in Reaction Centers from Rhodobacter sphaeroides Revealed by Femtosecond Transient Absorption. *J. Phys. Chem. B* **2009**, 113 (31), 11023-11031.

(21) McAuley-Hecht, K. E.; Fyfe, P. K.; Ridge, J. P.; Prince, S. M.; Hunter, C. N.; Isaacs, N. W.; Cogdell, R. J.; Jones, M. R. Structural Studies of Wild-Type and Mutant Reaction Centers from an Antenna-Deficient Strain of Rhodobacter sphaeroides: Monitoring the Optical Properties of the Complex from Bacterial Cell to Crystal. *Biochemistry*, **1998**, 37 (14), 4740-4750.

(22) Pelant, I.; Valenta, J. *Luminescence Spectroscopy of Semiconductors*; Oxford University Press, Oxford, 2012.

(23) Fajer, J.; Brune, D. C.; Davis, M. S.; Forman, M.; Spaulding, L. D. Primary Charge Separation in Bacterial Photosynthesis: Oxidized Chlorophylls and Reduced Pheophytin. *Proc. Natl. Acad. Sci. U.S.A.* **1975**, 72 (12), 4956-4960.
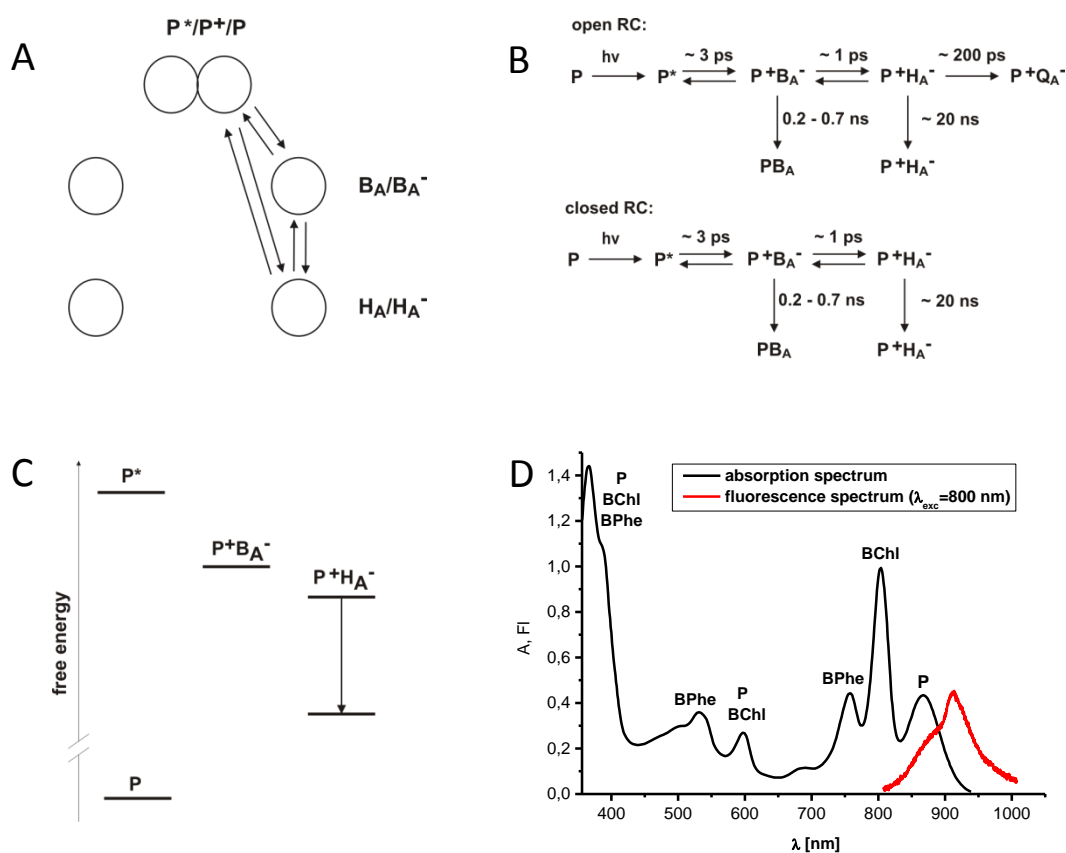
Fig. 1. Structure, electron transfer reactions, energetic diagram, and spectra of *Rba. sphaeroides* RCs. A – cartoon of the structural arrangement of the electron transfer cofactors; reversible electron transfer reactions are represented by the arrows. B – electron transfer reactions schemes for open and closed RCs. C – simplified free energy diagram of RC cofactor states; the arrow represents temporal evolution of the free energy level of $P^+H_A^-$. D – steady state absorption and fluorescence spectra of *Rb. sphaeroides* RCs; absorption bands are labeled according to the contribution of particular cofactors; the fluorescence spectrum was measured with an excitation wavelength of 800 nm.
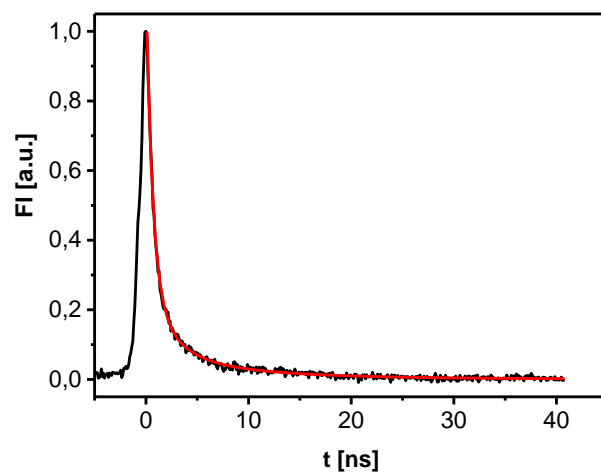
Fig. 2. Decay of fluorescence integrated over the central part of the emission band of P between ~920 and ~940 nm. The best three-exponential fit is shown in red and superimposed on the data. The best fit parameters were $\tau_1 = 0.63 \pm 0.03$ ns ($F_1 = 0.73$), $\tau_2 = 2.4 \pm 0.6$ ns ($F_2 = 0.20$), $\tau_3 = 9.6 \pm 2.5$ ns ($F_3 = 0.07$).
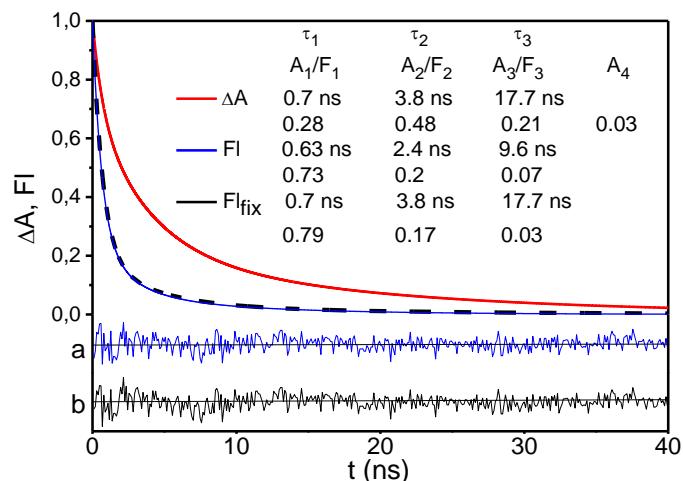
	τ_1	τ_2	τ_3	
	A_1/F_1	A_2/F_2	A_3/F_3	A_4
ΔA	0.7 ns	3.8 ns	17.7 ns	
	0.28	0.48	0.21	0.03
Fl	0.63 ns	2.4 ns	9.6 ns	
	0.73	0.2	0.07	
Fl$_{fix}$	0.7 ns	3.8 ns	17.7 ns	
	0.79	0.17	0.03	

Fig. 3. Comparison of fits to absorbance changes at 690 nm from ref. 11 and to the fluorescence decay trace from Fig. 2, both revealing $P^+H_A^-$ charge recombination. The fluorescence decay was fitted with a three-exponential function (blue), whereas absorption changes were fitted with three-exponential function plus a small constant due to triplet state formation (red). A second fit of the fluorescence decay is shown (dashed black) with three fixed lifetimes taken from previous transient absorption studies.[11] Residuals (a) and (b) of the two fits to the fluorescence decay curve are shown. Note that the difference between the two fluorescence fits is smaller than the width of the lines.
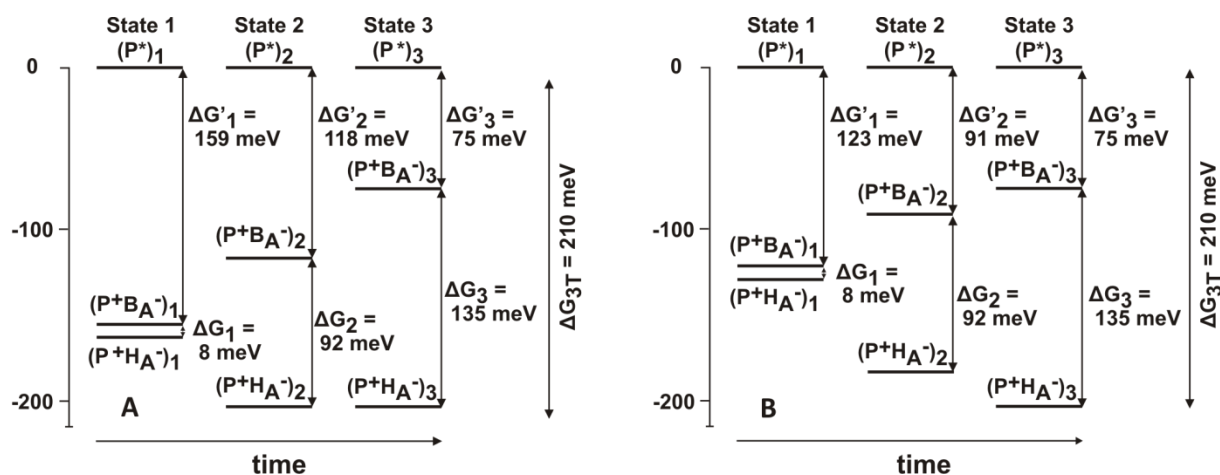
Fig. 4. Temporal evolution of the free energy of states $P^+B_A^-$ and $P^+H_A^-$ relative to that of P^*. The value of $\Delta G_{3T} = 210$ meV was fixed and taken from ref. 3, and those for ΔG_1, ΔG_2, ΔG_3 were taken from ref. 11. $\Delta G_3'$ was calculated as a difference $\Delta G_{3T} - \Delta G_3$. (A) $\Delta G_1'$ and $\Delta G_2'$ were estimated on the basis of parameters F_1, F_2, F_3 and τ_1, τ_2, τ_3 of the best fit to fluorescence decay (Fig. 3 – residuals a; and Tab. 2, col. 4). (B) $\Delta G_1'$ and $\Delta G_2'$ were estimated on the basis of parameters F_1, F_2, F_3 and τ_1, τ_2, τ_3 estimated from the fit in which τ_1, τ_2, and τ_3 were fixed and taken from the transient absorption studies[11] (Fig. 3 – residuals b; and Tab. 2, col. 5).

Table 1. Fit parameters of fluorescence and absorption kinetics depicting $P^+H_A^-$ charge recombination and model parameters depicting protein dynamics.

|	Fit parameters									Model parameters
Set	Fluorescence				Absorption					Absorption
	τ_1[ns] F_1	τ_2[ns] F_2	τ_3[ns] F_3	τ_{av}[ns]	τ_1[ns] A_1	τ_2[ns] A_2	τ_3[ns] A_3	A_4	τ_{av}[ns]	τ_{12}[ns] τ_{23}[ns]
A	0.63 0.73	2.4 0.2	9.6 0.07	1.61	————					———
B	0.7 0.79	3.8 0.17	17.7 0.03	1.73	————					———
C	0.7 0.8	4.0 0.16	14.0 0.03	1.62	————					———
D	0.67 0.62	3.2 0.27	10.6 0.11	2.45	————					———
E	0.7 0.63	3.8 0.3	17.7 0.07	2.82	————					———
F	————				0.7 0.28	3.8 0.48	17.7 0.21	0.03	5.74	0.55 10
G	————				0.7 0.26	4.0 0.60	14.0 0.11	0.03	4.12	———

The fit parameters were taken from the following studies: (A) our measurement, free fit; (B) our measurement; lifetimes fixed - taken from transient absorption experiment;[11] (C) our measurement; lifetimes fixed - taken from transient absorption experiment;[20] (D) ref. 19; (E) experimental decay taken from ref. 19; lifetimes fixed - taken from transient absorption experiment;[11] (F) ref. 11; (G) ref. 20. The sets A and B correspond to fits, the residuals of which are shown in Fig. 3 and are labeled a and b, respectively.

Table 2. Probabilities of population of states P*, $P^+B_A^-$ and $P^+H_A^-$ and free energy gaps between these states in three protein relaxation states of isolated RCs from *Rba. sphaeroides* for four sets of fluorescence decay parameters used in model calculations.

Probabilities of population and free energy gaps symbols	States of cofactors	State of protein	Probabilities of population and free energy gaps [eV] values for four input sets of fluorescence decay parameters, A-D			
			A	B	C	D
			$\tau_1 = 0.63$ [ns] $\tau_2 = 2.4$ [ns] $\tau_3 = 9.6$ [ns] $F_1 = 0.73$ $F_2 = 0.2$ $F_3 = 0.07$	$\tau_1 = 0.7$ [ns] $\tau_2 = 3.8$ [ns] $\tau_3 = 17.7$ [ns] $F_1 = 0.79$ $F_2 = 0.17$ $F_3 = 0.03$	$\tau_1 = 0.7$ [ns] $\tau_2 = 4$ [ns] $\tau_3 = 14$ [ns] $F_1 = 0.8$ $F_2 = 0.16$ $F_3 = 0.03$	$\tau_1 = 0.67$ [ns] $\tau_2 = 3.2$ [ns] $\tau_3 = 10.6$ [ns] $F_1 = 0.62$ $F_2 = 0.27$ $F_3 = 0.11$
1	2	3	4	5	6	7
P_1''	$(P^*)_1$	unrelaxed state state 1	0,000875	0.00349	0.00391	0.000902
P_1'	$(P^+B_A^-)_1$		0.423	0.422	0.422	0.423
P_1	$(P^+H_A^-)_1$		0.576	0.574	0.574	0.576
$\Delta G_1'$ [eV]	$(P^*)_1 - (P^+B_A^-)_1$		0.159	0.123	0.12	0.159
ΔG_1 [eV]	$(P^+B_A^-)_1 - (P^+H_A^-)_1$		*0.008*	*0.008*	*0.008*	*0.008*
ΔG_{1T} [eV]	$(P^*)_1 - (P^+H_A^-)_1$		0.167	0.131	0.128	0.167
P_2''	$(P^*)_2$	partially relaxed state state 2	0.000292	0.000818	0.000874	0.000415
P_2'	$(P^+B_A^-)_2$		0.0282	0.0282	0.0282	0.0286
P_2	$(P^+H_A^-)_2$		0.972	0.971	0.971	0.971
$\Delta G_2'$ [eV]	$(P^*)_2 - (P^+B_A^-)_2$		0.118	0.091	0.089	0.110
ΔG_2 [eV]	$(P^+B_A^-)_2 - (P^+H_A^-)_2$		*0.092*	*0.092*	*0.092*	*0.092*
ΔG_{2T} [eV]	$(P^*)_2 - (P^+H_A^-)_2$		0.21	0.183	0.181	0.202
P_3''	$(P^*)_3$	fully relaxed state state 3	0.000279	0.000279	0.000279	0.000279
P_3'	$(P^+B_A^-)_3$		0.00519	0.00519	0.00519	0.00519
P_3	$(P^+H_A^-)_3$		0.995	0.995	0.995	0.995
$\Delta G_3'$ [eV]	$(P^*)_3 - (P^+B_A^-)_3$		0.075	0.075	0.075	0.075
ΔG_3 [eV]	$(P^+B_A^-)_3 - (P^+H_A^-)_3$		*0.135*	*0.135*	*0.135*	*0.135*
ΔG_{3T} [eV]	$(P^*)_3 - (P^+H_A^-)_3$		*0.21*	*0.21*	*0.21*	*0.21*

The symbols used are further explained in Fig. 4 and in the Supporting Information. The sets A-D correspond to those depicted in the footnote to Tab. 1. The values of free energy gaps between the states $P^+B_A^-$ and $P^+H_A^-$ were taken from ref. 11, and ΔG_{3T} was fixed at 0.21 eV.[3] The remaining values (typed in bold) were estimated from the expressions shown in the Supporting Information.

TOC graphic

time, protein polarity near B_A and H_A
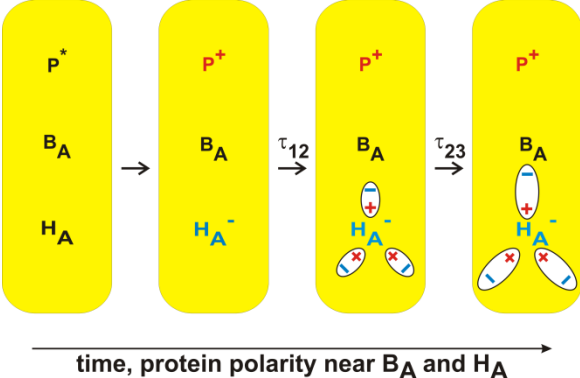
Supporting Information

In order to estimate the free energy gaps between P* and the charge separated states we used the model presented graphically in Fig. A1. This is an extension of a previous model[11] which did not allow estimation of the free energy levels of the state P*.
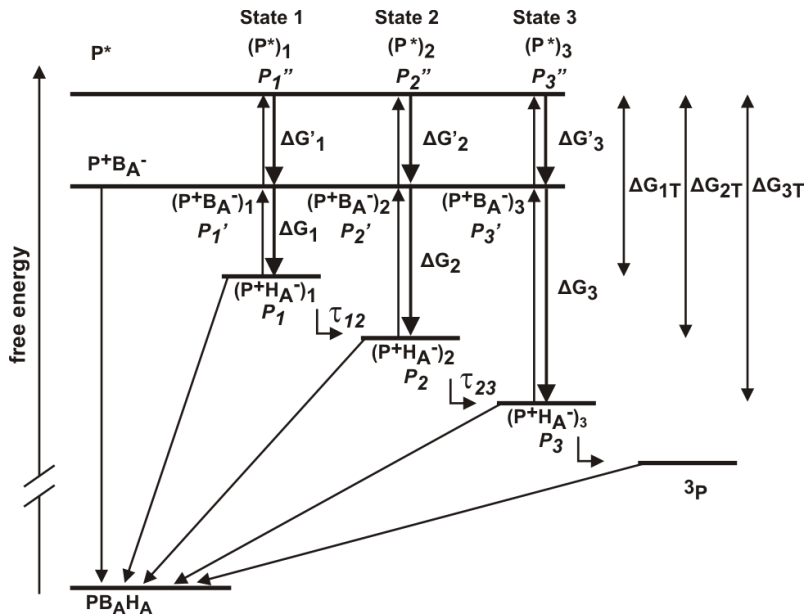

Fig. A1. Working model used for calculations. See text for details.

We assumed that the RCs consecutively adopt three states numbered by index i = 1 .. 3 (Fig. A1). Furthermore, we assume that the transitions between these states are irreversible (characterized by time constants τ_{12} and τ_{23}) and in each of these states an equilibrium between exited, $(P^*)_i$, and charge separated, $(P^+B_A^-)_i$, and $(P^+H_A^-)_i$, states is established. P_i'', P_i', and P_i denote equilibrium probabilities of population of the states $(P^*)_i$, $(P^+B_A^-)_i$, and $(P^+H_A^-)_i$, respectively. In the equilibrium states:

$$\frac{P_i''}{P_i'} = e^{-\frac{\Delta G_i'}{kT}} \tag{A1}$$

$$\frac{P_i'}{P_i} = e^{-\frac{\Delta G_i}{kT}} \tag{A2}$$

$$\frac{P_i''}{P_i} = \frac{P_i''}{P_i'} \cdot \frac{P_i'}{P_i} = e^{-\frac{\Delta G_i'}{kT}} \cdot e^{-\frac{\Delta G_i}{kT}} = e^{-\frac{(\Delta G_i' + \Delta G_i)}{kT}} = e^{-\frac{\Delta G_{iT}}{kT}} \tag{A3}$$

where k is the Boltzman factor, T is absolute temperature, and free energy gaps ΔG_i, $\Delta G_i'$, and ΔG_{iT} are explained in Fig. A1. The probabilities are normalized:

$$P_i + P_i' + P_i'' = 1 \tag{A4}$$

From the eqn. A1- A4 one can show that:

$$P_i'' = \frac{e^{-\frac{\Delta G_{iT}}{kT}}}{1 + e^{-\frac{\Delta G_i}{kT}} + e^{-\frac{\Delta G_{iT}}{kT}}} \tag{A5}$$

$$P_i' = \frac{e^{-\frac{\Delta G_i}{kT}}}{1 + e^{-\frac{\Delta G_i}{kT}} + e^{-\frac{\Delta G_{iT}}{kT}}} \tag{A6}$$

$$P_i = \frac{1}{1 + e^{-\frac{\Delta G_i}{kT}} + e^{-\frac{\Delta G_{iT}}{kT}}} \tag{A7}$$

The state ^3P in Fig. A1 is the triplet state of the primary donor. Since we did not observe non-decaying component in fluorescence decay traces, it was assumed in the model that the formation of the triplet state did not affect the fluorescence kinetics unlike the transient absorption kinetics.

Calculations for state 3 (relaxed state)

The ΔG_{3T} values found in the literature range from 0.21 eV to 0.26 eV [3] and the value of ΔG_3 was proposed to be 0.135 eV.[11] After introducing these values to Eqn. A1-A4 (for i = 3), one may calculate probabilities P_3, P_3', and P_3''. The free energy gap $\Delta G_3'$ is simply calculated as difference between ΔG_{3T} and ΔG_3.

Calculations for states 1 and 2 (unrelaxed and partially relaxed states)

Fluorescence amplitudes F_1-F_3 (see Tab. 1) are complex functions of time constants τ_{12} and τ_{23}, rate constants k_{PHi} (i = 1,2,3) and probabilities p_i'' (i = 1, 2, 3) and P_1 .

$$F_1 = p_1'' + p_2'' \frac{\tau_{12}^{-1} P_1}{k_{PH2} - k_{PH1}} + p_3'' \frac{\tau_{12}^{-1} P_1}{k_{PH2} - k_{PH1}} \frac{\tau_{23}^{-1}}{k_{PH3} - k_{PH1}} \tag{A8}$$

$$F_2 = -\left(p_2'' \frac{\tau_{12}^{-1} P_1}{k_{PH2} - k_{PH1}} + p_3'' \frac{\tau_{12}^{-1} P_1}{k_{PH2} - k_{PH1}} \frac{\tau_{23}^{-1}}{k_{PH3} - k_{PH1}} \right) \tag{A9}$$

$$F_3 = -p_3'' \frac{\tau_{12}^{-1} P_1 \tau_{23}^{-1}}{k_{PH2} - k_{PH1}} \left[\frac{1}{k_{PH3} - k_{PH1}} \frac{1}{k_{PH3} - k_{PH2}} \right] \tag{A10}$$

Time constants τ_{12} and τ_{23} are shown in Fig. A1 and depict two phases of protein reorganization dynamics. Rate constants k_{PH1}, k_{PH2}, and k_{PH3} are the inverted lifetimes τ_1, τ_2, τ_3 of the states $(P^+H_A^-)_1$, $(P^+H_A^-)_2$, and $(P^+H_A^-)_3$, respectively, achieved from the fit of fluorescence decay. p_1'', p_2'', and p_3'' are equilibrium probabilities of population of the states $(P^*)_1$, $(P^*)_2$, and $(P^*)_3$, respectively. Note that the probabilities p_1'', p_2'', p_3'' do not fulfill the normalization condition similar to A4 (for example $p_1'' + p_1' + p_1 \neq 1$). Their exact values originate from another normalization condition:

$$F_1 + F_2 + F_3 = 1 \tag{A11}$$

However, the ratios between probabilities p_i, p_i', and p_i'' (i=1, 2, 3) are the same as the respective ratios between probabilities P_i, P_i', P_i'' and therefore also fullfil the eqn. A1-A3:

$$\frac{p_i''}{p_i'} = e^{-\frac{\Delta G_i'}{kT}} \tag{A12}$$

$$\frac{p_i'}{p_i} = e^{-\frac{\Delta G_i}{kT}} \tag{A13}$$

$$\frac{p_i''}{p_i} = e^{-\frac{\Delta G_{iT}}{kT}} \tag{A14}$$

Eqn. A8-A10 were derived from a set of differential equations depicting temporal evolution of the concentrations of states P^*, $P^+B_A^-$ and $P^+H_A^-$ in a similar way as was done for absorption amplitudes.[11]

Eqn. A8-A10 allow the calculation of probabilities p_1'', p_2'', and p_3'', taking the values of time constants τ_{12} and τ_{23} from ref. 11 and taking the lifetimes $\tau_1 = \frac{1}{k_{PH1}}$, $\tau_2 = \frac{1}{k_{PH2}}$, and $\tau_3 = \frac{1}{k_{PH3}}$, and amplitudes F_1, F_2, and F_3 from one of the sets of fluorescence parameters (Tab. 1, sets A-E).

Knowing the values of P_3, P_3', P_3'' (see above calculations, for state 3), p_1'', p_2'', and p_3'' (Eqn. A8- A10), taking the values of ΔG_1= 0.008 eV and ΔG_2=0.92 eV from transient absorption measurements,[11] and using Eqn. A1-A3 and A12-A14 one may calculate $\Delta G_1'$ and $\Delta G_2'$.